Single-Phase Improved Active Clamp Coupled-Inductor-Based Converter With Extended Voltage Doubler Cell

Yi Zhao, *Student Member, IEEE*, Wuhua Li, *Member, IEEE*, and Xiangning He, *Fellow, IEEE*

***Abstract*—In this paper, A single-phase improved active clamp coupled-inductor-based converter with extended voltage doubler cell is proposed for large-voltage conversion ratio applications. The secondary winding of the coupled inductor is inserted into the half-wave voltage doubler cell to extend the voltage gain dramatically and decrease the switch voltage stress effectively. By combining the coupled inductor and voltage doubler cell structure, the disadvantage of the potential resonance between the leakage inductance and the diode stray capacitor is cancelled, and the unexpected high pulsed current in the voltage doubler cell is decreased due to the inherent leakage inductance of the coupled inductor. Meanwhile, the active clamp scheme is employed to recycle the leakage energy, suppress the switch turn-off voltage spikes, and implement zero-voltage-switching turn-on operation. In addition, there is only one magnetic component in the proposed converter and the coupled inductor operates not only as a filter inductor, but also as a transformer when the main switch is in the ON state, which reduces the volume of the magnetic core and improves the power density of the converter. A 500 W prototype operating at 100 kHz with 48 V input and 380 V output is built to verify the analysis. The maximum efficiency of the prototype is nearly 97% and the efficiency is higher than 96% over a wide load range.**

***Index Terms*—Coupled inductor and voltage doubler, high step-up, switched capacitor.**

I. Introduction

In recent years, with the rapid increase in energy demand, much attention has been paid to photovoltaic (PV) generation systems. In the grid-connected PV generation systems, PV panels are usually connected in series to directly obtain a high-bus voltage to supply the grid. Sometimes, a conventional boost converter is applied to improve the maximum power point track (MPPT) range of the systems. However, if the *V–I* characteristics of the PV panels lack consistency, not all the PV panels operate under the best condition. For instance, when partial shading happens, the MPPT losses are increased considerably [1], [2]. Modular systems are introduced to improve the system MPPT efficiency. For example, as shown in Fig. 1, an independent module-integrated converter is used for each PV panel to transfer the energy to the grid. Thus, every PV panel is decoupled with others, which makes the system configuration flexible and maximizes the output power. Usually, the module-integrated converter has a dc–dc stage and a dc–ac stage, and one of the main challenges in this system is how to convert the low voltage of the PV array to a high one with high efficiency [3], [4]. Unfortunately, the conventional boost converter is not suitable for high step-up conversion applications. First, the high conversion ratio calls for high duty cycle, which results in large conduction losses on the power device due to the large peak current. Moreover, the voltage stress of the switch is equal to the high output voltage, which makes only high on-resistance switch to be used, which generates high conduction losses. In addition, the switch and the diode operate under hard switching condition, which leads to large switching losses [5]–[7].

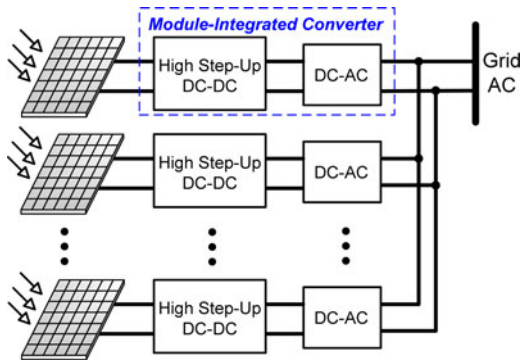

Fig. 1. Module-integrated converter-based grid-connected PV system.

To achieve a high conversion ratio and avoid operating at extremely high duty cycles, transformer-based converters are usually chosen. Many isolated current-fed converters, such as the current-fed push–pull converters [8], the current-fed full-bridge converters [9], and the dual boost converters [10], [11], are applied in high-conversion ratio applications. Compared with the voltage-fed converters, the voltage stresses of the rectifier diodes and the turns ratio of the transformer are reduced in the current-fed converters due to their boost-type configuration, which make them more suitable to obtain a high-voltage gain [12], [13]. However, the driving circuits and the sampling circuits in the isolated converters may increase the system complexity and the

Manuscript received May 23, 2011; revised November 9, 2011; accepted November 9, 2011. Date of current version March 16, 2012. This work was supported by the National Nature Science Foundation of China under Grant 50907058, the Zhejiang Province Science and Technology Program under Grant 2011C21056, and the Power Electronics Science and Education Development Program of Delta Environmental & Educational Foundation under Grant DREG2011002. Recommended for publication by Associate Editor B. Lehman.

The authors are with the National Laboratory of Power Electronics, College of Electrical Engineering, Zhejiang University, Hangzhou 310027, China (e-mail: diabloturen@zju.edu.cn; woohualee@zju.edu.cn; hxn@zju.edu.cn).

Color versions of one or more of the figures in this paper are available online at http://ieeexplore.ieee.org.

Digital Object Identifier 10.1109/TPEL.2011.2176752

cost compared with those in the nonisolated converters. Moreover, one inductor and one transformer are required at the very least in these converters, which increases the circuit volume and reduces the power density.

Another method for extending the voltage gain is to use switched capacitor or switched inductor technology. With switched capacitor technology, the conversion ratio of the converter is increased and the voltage stresses of the devices are reduced [14]. Additionally, a small resonant inductor is added into the switched capacitor circuit to solve the diode reverse-recovery problem and depress the large pulsed current across the switches when they turn ON [15], [16]. However, when the conversion ratio is extremely large, many switched capacitor stages are required to achieve the high voltage gain, which makes the circuit complex. Switched inductor technology is also helpful for increasing the conversion ratio [17]. Unfortunately, the voltage stresses of the switches in these two types of converters are still high, thus the high-voltage rated switch causes serious conduction losses. The switched capacitor and the switched inductor are combined together to extend the voltage gain greatly and reduce the switch voltage stresses significantly [18], [19]. Unfortunately, the negative ports of the input and output sides are not connected, which may cause large earth leakage current in grid-connected systems.

The problems existing in the conventional boost converter working under the high step-up condition can be solved by introducing a coupled inductor [20]. The voltage gain is extended and the voltage stress on the switch is reduced. Moreover, only one magnetic component is used, which reduces the volume and the complexity of the converter. However, the leakage inductance of the coupled inductor may not only cause high voltage spikes on the switch when it turns OFF, but also induce large energy losses. A resistor–capacitor–diode (RCD) snubber can suppress the voltage stress of the switch, but the leakage energy is dissipated. A passive lossless clamp circuit composed of a diode and a capacitor is added to clamp the turn-off voltage spikes on the switch and recycle the leakage inductance energy [21]. Thus, the low-voltage rated switches can be employed to improve the efficiency. Meanwhile, the reverse-recovery problem of the output diode is partly solved by the reasonable design of the leakage inductance. Furthermore, many other high step-up converters with coupled inductors technology and passive lossless clamp have been proposed in the recent years [22]–[25]. However, the switches in these converters work under hard switching condition.

As shown in Fig. 2, an active clamp coupled-inductor-based converter (ACCIB converter) is proposed, in which the active clamp scheme is introduced to replace the passive lossless clamp circuit and achieve similar function [26]. In this converter, both the main and auxiliary switches turn ON under zero-voltage-switching (ZVS) condition. And the turn-off losses of the two switches are reduced greatly due to the parallel capacitors C_{s1} and C_{s2}. Therefore, ACCIB converter is an acceptable candidate for high step-up applications. Unfortunately, the voltage stress of the output diode in ACCIB converters is higher than its output voltage. Also the resonance between the leakage inductance and the stray capacitor of the output diode causes some electro-

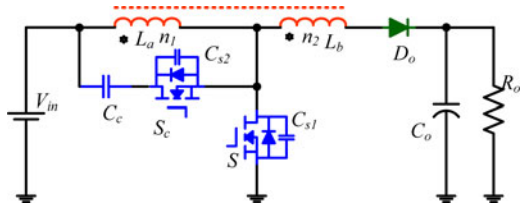

Fig. 2. Active clamp coupled-inductor-based converter in [26].

magnetic interference problems and further increases the output diode voltage stress. Therefore, an additional RCD snubber has to be employed to mitigate this problem.

In this paper, a novel single-phase improved ACCIB converter with an extended voltage doubler cell is proposed to fulfill high step-up requirements and solve the inevitable problems existing in the ACCIB converter. Compared with the ACCIB converter, a small capacitor and diode are added. The proposed converter has the same advantages as those previously mentioned for the ACCIB converter. Besides, the voltage stress of the output diode is reduced and the resonance between the leakage inductance and the stray capacitor of the output diode is eliminated. In addition, a higher conversion ratio is obtained due to the added switched capacitor. Moreover, when the main switch is in the ON state, the coupled inductor transfers the energy like a transformer. When the main switch is in the OFF state, the coupled inductor transfers the energy as a filter inductor. Therefore, the volume of the magnetic material is reduced due to the full utilization of the coupled inductor.

This paper is organized as follows. The circuit introduction and its steady-state operational analysis are given in Section II. The circuit performance analysis is discussed in Section III. Three novel converters derived from the proposed extended voltage doubler cell are given in Section IV. The experimental results of a 500 W 48 V-input 380 V-output prototype with 100 kHz switching frequency are shown in Section V to verify the analysis. A valuable summary is given in the final section.

II. Proposed Converter and Operation Analysis

The proposed single-phase improved ACCIB with the extended voltage doubler cell is illustrated in Fig. 3(a). A conventional boost converter can be obtained by removing the components in the dashed blocks, including a main switch S, an output diode D_o, an inductor L_a, an output capacitor C_o, and the load R_o. The clamp circuit is marked in the rectangular block, which is composed of an auxiliary switch S_c and a capacitor C_c. The extended voltage doubler cell circuit is plotted in the elliptical block, composed of an inductor L_b, a switched capacitor C_m, and a regenerative diode D_r. The inductor L_a is coupled to the inductor L_b. The coupling reference is marked by "$*$."

The coupled inductor can be considered as an ideal transformer, a parallel magnetizing inductance L_m, and a series leakage inductance L_{Lk} [21]. The equivalent circuit of the coupled inductor is shown in Fig. 3(b). L_a and L_b represent the primary and the secondary windings, respectively. N is the turns

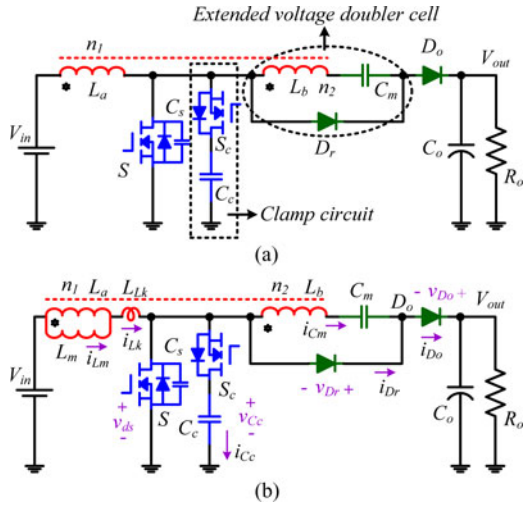

Fig. 3. Proposed single-phase high step-up ZVT boost converters with improved voltage gain extension cell and equivalent circuit of coupled inductor. (a) Proposed converter. (b) Equivalent circuit of coupled inductor.

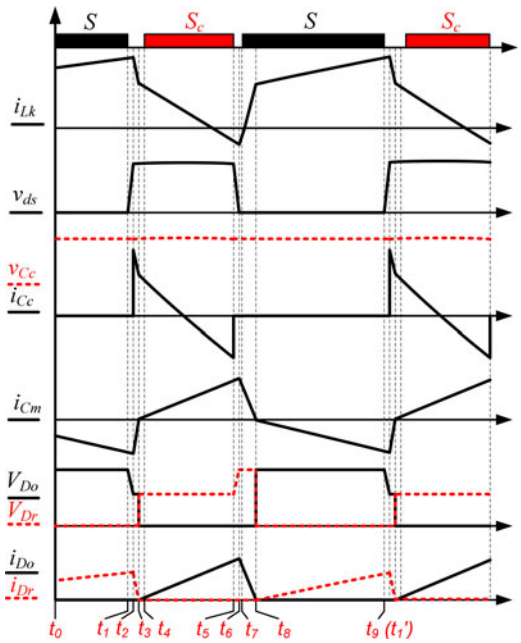

Fig. 4. Key waveforms of proposed converter.

ratio n_2/n_1. C_s is the parallel capacitor to achieve zero-voltage-transition (ZVT) performance, which includes the parasitic capacitors of the main and clamp switches.

There are eight main subintervals during one switching cycle. The key waveforms are shown in Fig. 4. The explanation of each waveform is given as follows: i_{Lk} is the current through leakage inductance L_{Lk}, also it is the input current of the converter; v_{ds} is the voltage across main switch S; v_{Cc} is the voltage across clamp capacitor C_c; i_{Cc} is the current though clamp circuit S_c and C_c; i_{Cm} is the current through switched capacitor C_m; v_{Do}, v_{Dr}, i_{Do}, and i_{Dr} are the voltages and currents of diodes D_o and D_r. The equivalent circuits for each subinterval are shown in Fig. 5.

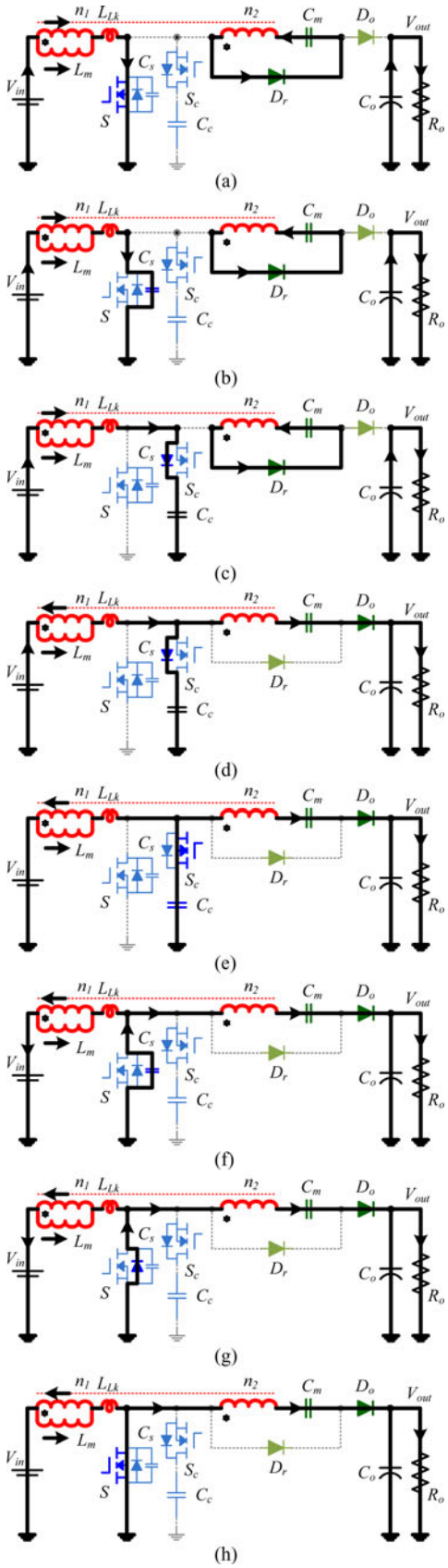

Fig. 5. Operation processes of proposed converter. (a) Subinterval 1 [t_0–t_1]. (b) Subinterval 2 [t_1–t_2]. (c)Subinterval 3 [t_2–t_3]. (d) Subinterval 4 [t_3–t_4]. (e) Subinterval 5 [t_4–t_5]. (f) Subinterval 6 [t_5–t_6]. (g) Subinterval 7 [t_6–t_7]. (h) Subinterval 8 [t_7–t_8].

A. Subinterval 1 [t_0–t_1]

Before t_1, main switch S is in the ON state while clamp switch S_c is in the OFF state. During this period, output diode D_o is antibiased. Magnetizing inductance L_m is charged by input voltage $V_{\rm in}$, thus the magnetizing current increases gradually almost in a linear way. At the same time, the energy is transferred to switched capacitor C_m by the coupled inductor. The current through the secondary winding is limited by leakage inductance L_{Lk}. The currents through L_m and L_{Lk} are given by

$$i_{Lm}(t) = I_{Lm}(t_0) + \frac{V_{\rm in}}{L_m}\cdot(t-t_0) \tag{1}$$

$$i_{Lk}(t) \approx i_{Lk}(t_0) + \frac{V_{\rm in} - V_{Cm}/N}{L_{Lk}}\cdot(t-t_0). \tag{2}$$

B. Subinterval 2 [t_1–t_2]

Main switch S turns OFF at t_1, then parallel capacitor C_s begins to resonante with leakage inductance L_{Lk}. Because C_s is small and L_{Lk} is relatively large, the voltage v_{ds} on main switch S rises almost at a constant slope from zero. The turn-off losses of the main switch are reduced due to the existence of C_s

$$v_{ds}(t) \approx \frac{I_{Lk}(t_1)}{C_s}\cdot(t-t_1). \tag{3}$$

C. Subinterval 3 [t_2–t_3]

At t_2, the switching voltage of the main switch reaches the clamp capacitor voltage, and the antiparallel diode of clamp switch S_c is forced to conduct. Then v_{ds} is clamped to v_{Cc} by the antiparallel diode of clamp switch S_c. Since clamp capacitor C_c is much larger than C_s, C_s can be neglected and almost all the current flow through C_c. After t_2, leakage inductance L_k is discharged by the voltage of $V_{\rm in}-V_{cm}/N-V_{Cc}$. As shown in (4), compared with $-V_{Cc}$, the voltage of $V_{\rm in}-V_{Cm}/N$ is much smaller and it can be neglected to simplify the expression. In this short subinterval, the current through L_{Lk} decreases approximately linearly, as well as the current through the secondary winding

$$\begin{aligned} i_{Lk}(t) &= I_{Lk}(t_2) + \frac{V_{\rm in} - V_{Cm}/N - V_{Cc}}{L_{Lk}}(t-t_2) \\ &\approx I_{Lk}(t_2) - \frac{V_{Cc}}{L_{Lk}}(t-t_2). \end{aligned} \tag{4}$$

D. Subinterval 4 [t_3–t_4]

The voltage across output diode D_o falls to zero at t_3, then the energy stored in L_m and C_m begins to be transferred to the load. L_m is discharged during this period. Leakage inductance L_{Lk} begins to resonate with clamp capacitor C_c and switched capacitor C_m. Due to the relative large resonant period, the leakage inductance current reduces nearly linearly

$$i_{Lm}(t) = I_{Lm}(t_3) - \frac{[V_{\rm out} - V_{Cc} - V_{Cm}]}{N\cdot L_m}\cdot(t-t_3) \tag{5}$$

$$i_{Lk}(t) = I_{Lk}(t_3) - \frac{V_{Cc} - [V_{\rm out} - V_{Cm} - V_{Cc}]/N - V_{\rm in}}{L_{Lk}} \cdot(t-t_3). \tag{6}$$

E. Subinterval 5 [t_4–t_5]

The turn-on signal is applied to clamp switch S_c at t_4. S_c is turned ON when its body diode is conducting, thus the ZVS turn-on condition is achieved. The equivalent circuit in this subinterval is similar to that of subinterval 4.

F. Subinterval 6 [t_5–t_6]

Clamp switch S_c is turned OFF at t_6. After that, leakage inductance L_{Lk}, clamp capacitor C_c, and switched capacitor C_m stop resonating and a new resonance is formed by leakage inductance L_{Lk} and parallel capacitor C_s. Because C_s is small and L_{Lk} is relatively large, voltage on the main switch v_{ds} decreases almost at a constant slope while the voltage across clamp switch S_c increases from zero at the same rate. Thus, the turn-off losses of the main switch are reduced due to the existence of C_s

$$v_{ds}(t) \approx V_{Cc} + \frac{I_{Lk}(t_5)}{C_s}\cdot(t-t_5). \tag{7}$$

G. Subinterval 7 [t_6–t_7]

The voltage of parallel capacitor C_s falls to zero at t_6, and then the antiparallel diode of main switch S begins to conduct. C_s and L_{lk} stop resonating. The increasing rate of the current through L_{Lk} is controlled by the output voltage

$$i_{Lk}(t) = \frac{V_{\rm out} - V_{Cm} + N\cdot V_{\rm in}}{N\cdot L_{Lk}}\cdot(t-t_6) \approx \frac{V_{\rm out}}{N\cdot L_{Lk}}\cdot(t-t_6). \tag{8}$$

H. Subinterval 8 [t_7–t_8]

The turn-on signal is applied to main switch S when its antiparallel diode is in the ON state. Main switch S turns ON with ZVS. The equivalent circuit in this subinterval is similar to that of subinterval 7.

At t_8, the voltage of D_r drops to zero. After that L_m is charged by the input voltage and the energy is transferred to C_m by the coupled inductor again.

III. Circuit Performance Analysis

A. Voltage Gain

In the steady-state analysis, to simplify the analysis, the voltages across clamp capacitor C_c and switched capacitor C_m are considered to be constant. Also, the losses of the power devices are not considered.

When the leakage inductance is zero, one switching period can be separated into two sections. When the main switch is in the ON state, the magnetizing inductor is charged by the input voltage

$$V_{Lm\_\rm charge} = V_{\rm in}. \tag{9}$$

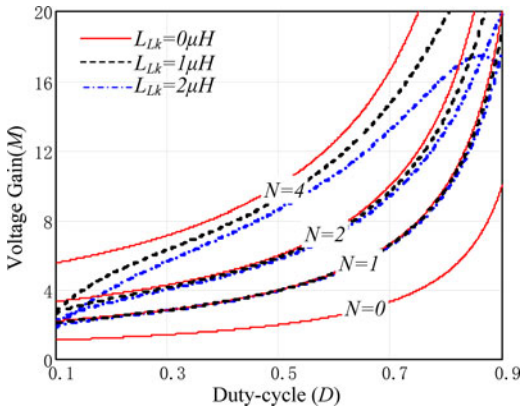

Fig. 6. Voltage gain of proposed converter.

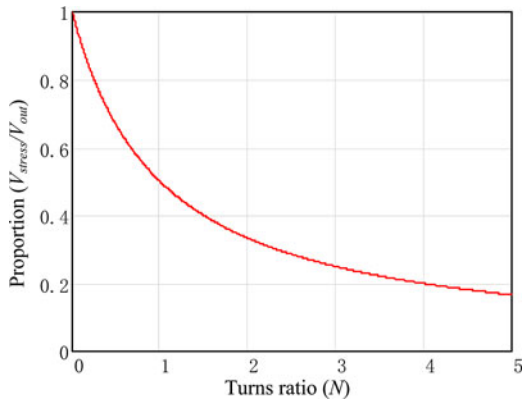

Fig. 7. Voltage stress reduction effect.

And the voltage of the switched capacitor can be expressed by

$$V_{Cm} = N \cdot V_{\text{in}}. \tag{10}$$

When the main switch is in the OFF state, the magnetizing inductor is discharged, and the voltage across the inductor can be derived by

$$V_{Lm\_\text{discharge}} = V_{Cc} - V_{\text{in}} = \frac{V_{\text{out}}}{N+1} - V_{\text{in}}. \tag{11}$$

By applying the inductor volt-second balance principle to the magnetizing inductor, the ideal voltage gain can be obtained by

$$M_{\text{ideal}} = \frac{V_{\text{out}}}{V_{\text{in}}} = \frac{N+1}{1-D}. \tag{12}$$

The operation analysis in the above section shows that the leakage inductance of the coupled inductor causes little duty-cycle loss. Considering the leakage inductance, the voltage gain of the proposed converter is expressed by

$$M = \frac{N+1}{1-D} \cdot \frac{1}{1 + 2 \cdot k_m \cdot N^2/D^2 + 2 \cdot k_m \cdot N^2/(1-D)^2} \tag{13}$$

where $k_m = L_{Lk} \cdot f_s / R_o \cdot f_s$ is the switching frequency. The detailed analysis is derived in the Appendix.

The relationship between the conversion ratio, the duty cycle, the leakage inductance, and the turns ratio are sketched in Fig. 6. When the turns ratio is zero, the voltage gain of the proposed converter is the same as that of the conventional boost converter. With increasing turns ratio, the voltage gain increases significantly. The leakage inductance affects the voltage gain of the converter a little. As the leakage inductance increases, the voltage gain decreases.

B. Voltage and Current Stresses

By neglecting the voltage ripple on the clamp capacitor, the voltage stress of the main switch can be derived from (10) and (11), which is given by

$$V_{\text{stress\_switch}} = \frac{V_{\text{in}}}{1-D} = \frac{V_{\text{out}}}{N+1}. \tag{14}$$

The voltage stress of the clamp switch is the same as that of the main switch. The proportion of the voltage stress and the output voltage with different turns ratios is plotted in Fig. 7. It can be seen that the voltage stress of the switch decreases sharply with increasing turns ratio. Thus, the high-performance switches can be used here to improve the efficiency. The RMS current of the main switch is given by

$$I_{\text{stress\_main}} = \frac{I_o}{1-D} \cdot \sqrt{\frac{(N^2+3) \cdot D^2 + (6N - 2N^2) \cdot D + 4N^2}{3 \cdot D}}. \tag{15}$$

The voltage stress of the diodes is equal to the output voltage. The voltage stress and the average current of the diodes are given by

$$V_{\text{stress\_diode}} = V_{\text{out}} \tag{16}$$

$$I_{\text{stress\_diode}} = I_o. \tag{17}$$

The voltage stress and RMS current of the added switched capacitor are given by

$$V_{\text{stress\_}Cm} = N \cdot V_{\text{in}} \tag{18}$$

$$I_{\text{stress\_}Cm} = 2 \cdot I_o \cdot \sqrt{\frac{1}{3D \cdot (1-D)}}. \tag{19}$$

C. Soft Switching Condition

The turn-off losses of both the main and clamp switches are reduced due to the parallel capacitor. The ZVS turn-on condition of the clamp switch can be realized by applying the turn-off signal to the clamp switch when its antiparallel diode is in the ON state during subinterval 6. To obtain the ZVS turn-on condition of the main switch, the energy stored in the leakage inductance should be larger than that stored in the parallel capacitor when the clamp switch turns OFF. Therefore, the voltage of the main switch can fall to zero before it turns ON. The ZVS-on condition is expressed in (20), and the equivalent expression is derived in

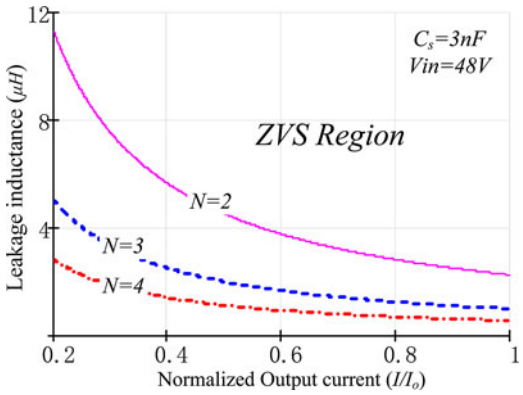

Fig. 8. ZVS soft switching condition with $V_{\rm in} = 48$ V and $C_s = 3$ nF.

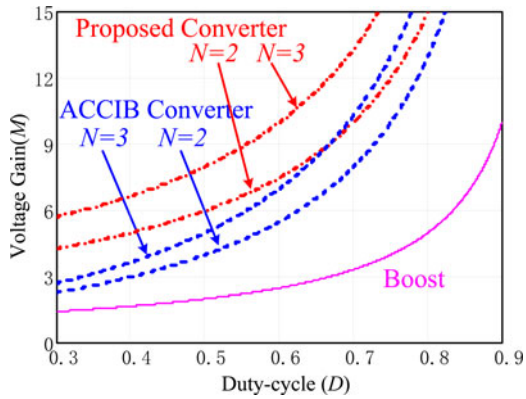

Fig. 9. Voltage gain comparison.

TABLE I
PERFORMANCE COMPARISON BETWEEN CONVENTIONAL BOOST CONVERTER, ACCIB CONVERTER, AND PROPOSED CONVERTER

Topology	Conventional Boost	ACCIB converter	The proposed converter
Active switches	1	2	2
Diodes	1	1	2
Voltage gain	*1/(1-D)*	*(1+N·D)/(1-D)*	*(1+N)/(1-D)*
Voltage stress of active switch	V_{out}	$V_{out}/(N{\cdot}D+1)$	$V_{out}/(N+1)$
Voltage stress of output diode	V_{out}	$(N+1){\cdot}V_{out}/(N{\cdot}D+1)$	V_{out}
Reverse recovery problem	Serious	Medium	Very small
Soft switching performance	Hard switching	ZVS	ZVS
Conduction losses	High	Medium	Medium
Switching losses	High	Low	Low

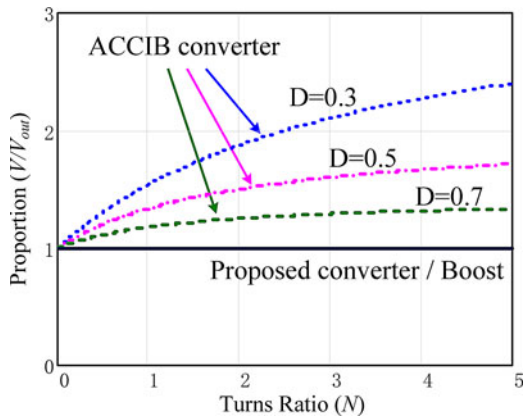

Fig. 10. Diode voltage stress comparison.

(21) for better understanding

$$L_k \cdot I_{Lk}(t_7)^2 \geq C_p \cdot V_{\rm mos}(t_7)^2 \tag{20}$$

$$L_{Lk} \cdot [(N-1) \cdot I_o]^2 \geq C_s \cdot V_{\rm in}^2. \tag{21}$$

The relationship between the leakage inductance and the output current to implement ZVS soft switching performance with $V_{\rm in} = 48$ V and $C_s = 3$ nF is illustrated in Fig. 8. When the turns ratio is lower than one, the ZVS turn-on condition of the main switch cannot be implemented. When the turns ratio is higher than one, as the output current increases, the leakage inductance required to realize ZVS soft switching condition decreases.

D. Performance Comparison

Table I shows the circuit performance comparison between the conventional boost converter, ACCIB converter, and the proposed converter. The proposed converter has one additional diode compared with the ACCIB converter. However, an extra RCD snubber is required in the ACCIB converter to eliminate the resonance between the leakage inductance and the stray capacitor of its output diode.

The relationships between the voltage gain and the duty cycle in the conventional boost converter, ACCIB converter, and the proposed converter are shown in Fig. 9. It can be seen that the ACCIB converter is a buck-boost-type converter while the proposed converter is a boost-type converter. Therefore, compared with the ACCIB converter, a lower turns ratio of the coupled inductor can be employed to realize the same conversion ratio, which helps reduce the copper losses and the leakage inductance of the coupled inductor.

The comparison of the output diode voltage stresses between the conventional boost converter, ACCIB converter, and the proposed converter is shown in Fig. 10. In the ACCIB converter, the voltage stress of the output diode is determined by the duty cycle and the turns ratio of the coupled inductor, and it is always higher than the output voltage. Fortunately, the voltage stress of the output diode in the proposed converter is the output voltage, which is the same as that in the conventional boost converter.

It is worth mentioning that one more step is required in the start-up process for the proposed converter compared to the conventional boost and ACCIB converters. In the proposed converter, before it works, the voltage on the switched capacitor C_m is zero. When the main switch turns ON, the voltage on C_m is charged by the input voltage through the coupled inductor. Therefore, some narrow pulse width signals should be applied to the switch, which helps to limit the possible inrush current. Fortunately, the leakage inductance can benefit to suppress the pulsed current during the start-up operation. Once the voltage

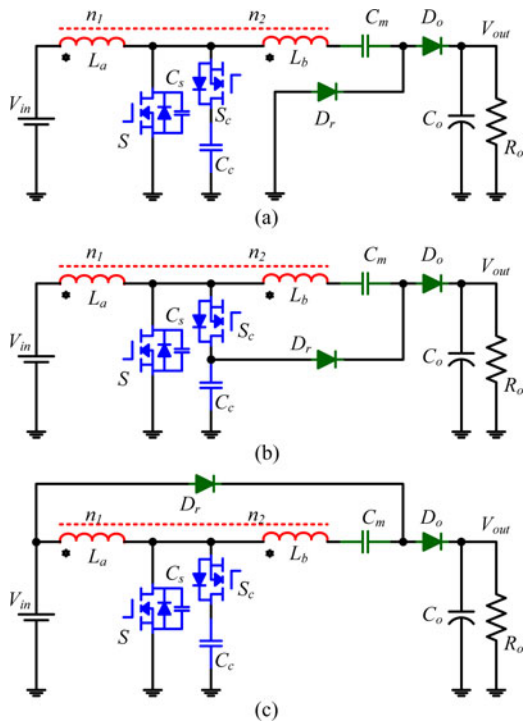

Fig. 11. Variations of proposed converter. (a) Converter A. (b) Converter B. (c) Converter C.

TABLE II
CIRCUIT PERFORMANCE COMPARISON

Topology	Proposed Converter	Converter A	Converter B	Converter C
Voltage gain	*(1+N)/(1-D)*	*(1+N)/(1-D)*	*(2+N)/(1-D)*	*(2+N-D)/(1-D)*
Voltage stress of switch	$V_{out}/(N+1)$	$V_{out}/(N+1)$	$V_{out}/(N+2)$	$V_{out}/(N+2-D)$
Voltage stress of diode	V_{out}	V_{out}	V_{out}	V_{out}

on C_m reaches $N{\cdot}V_{\rm in}$, the normal start-up control method can be used in the proposed converter.

IV. CIRCUIT VARIATIONS

As shown in Fig. 11, by changing the connection of the diode anode, three novel high step-up converters can be obtained with the similar circuit performance as the proposed converter, which are named Converter A, Converter B, and Converter C, respectively. In Fig. 11(a), when the main switch is in the ON state, the energy is transferred to switched capacitor C_m by the coupled inductor through switch S and regenerative diode D_r from the input source. In Fig. 11(b), when main switch S is in the ON state, the energy is transferred to C_m not only through the coupled inductor, but also through D_r from the input source directly. In Fig. 11(c), when main switch S is in the ON state, the energy is transferred to C_m from the input source through the coupled inductor and from clamp capacitor C_c through D_r. When main switch S is in the OFF state, the working processes of these three converters are similar to that of the proposed converter. A brief circuit performance comparison between the proposed converter and the three derived converters is given in Table II. It can be seen that the voltage gain of Converter A is the same as that of the proposed converter. The voltage gains of Converters B and C are both higher than that of the proposed converter. However, the current stresses of the main switches in these converters are larger than that of the proposed converter.

TABLE III
PARAMETERS OF PROTOTYPES

Converter	ACCIB converter	Proposed converter
Power Level	500W	500W
Input Voltage	40V~56V	40~56V
Output Voltage	380V	380V
Switching Frequency	100kHz	100kHz
Main Switch	IRFP4227Pbf	IRFP4227Pbf
Clamp Switch	IRFP4227Pbf	IRFP4227Pbf
Diodes	MUR15120	MUR1560
Clamp Capacitor	4.4μF	4.4μF
Parallel Capacitor	3.5nF	3.5nF
Switched Capacitor	NA	4.7μF
Output Capacitor	470μF	470μF
Turns Ratio	17:56	17:39
Magnetizing Inductance	88μH	88μH

V. EXPERIMENTAL RESULTS AND ANALYSIS

To demonstrate the effectiveness of the theoretical analysis, a 500 W prototype of the proposed converter is built and tested. At the same time, a 500 W prototype of the ACCIB converter is built as a comparison. The parameters of the converters are described in Table III. Generally, the size of the magnetic component accounts for a large proportion of the system volume. In the proposed converter, a Kool Mμ core with part number *KS*184-125*A* from Magnetic Company is used as the coupled inductors. The 3 mm^2 litzendraht wire is employed as the primary winding, and the 1 mm^2 litzendraht wire is adopted as the secondary winding. For the published ACCIB converter, the same core and litzendraht wires are applied to make a relatively fair performance comparison between these two converters. In fact, the coupled inductor in the proposed converter can deliver the energy to the load during the switch turn-on and turn-off stages. However, the coupled inductor in ACCIB converter stores its energy during the switch turn-on stage and releases the energy to the load during the switch turn-off stage. As a consequence, a smaller magnetic core can be applied in the proposed converter to reduce the size. The photograph of the coupled inductor in the proposed converter is shown in Fig. 12 to give a clear understanding of the main part of the converter.

Figs. 13–16 show the waveforms of the proposed converter at full load with 48 V input voltage. Fig. 17 is the waveform comparison between the proposed converter and the ACCIB converter.

The experimental waveforms of clamp capacitor voltage v_{Cc}, main switch voltage v_{ds}, and clamp capacitor current i_{Cc} are shown in Fig. 13. It can be seen that when the main switch

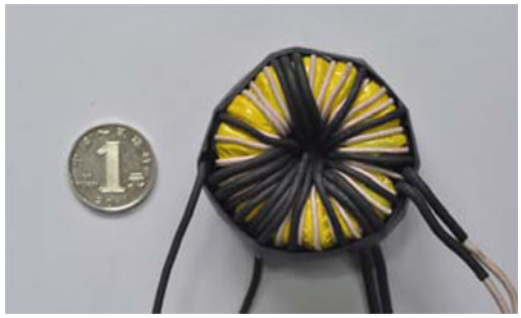

Fig. 12. Photograph of coupled inductor in proposed converter.

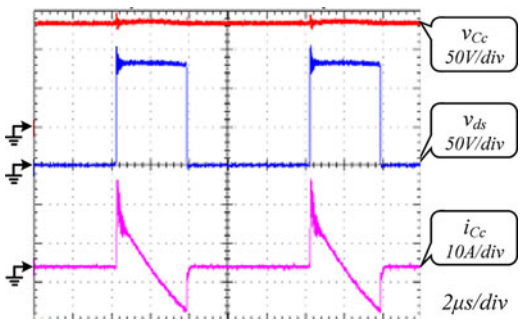

Fig. 13. Clamp circuit performance.

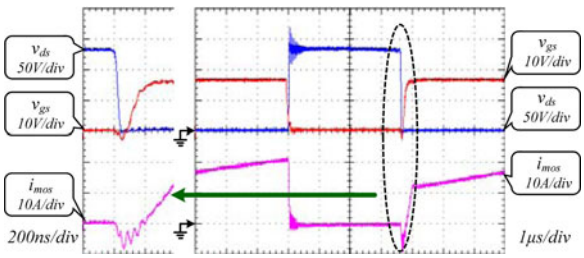

Fig. 14. ZVS-on performance of main switch.

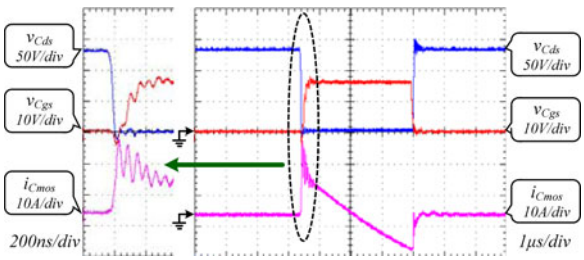

Fig. 15. ZVS-on performance of clamp switch.

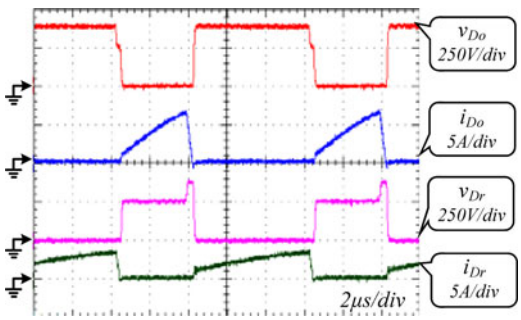

Fig. 16. Voltage and current waveforms of D_o and D_r.

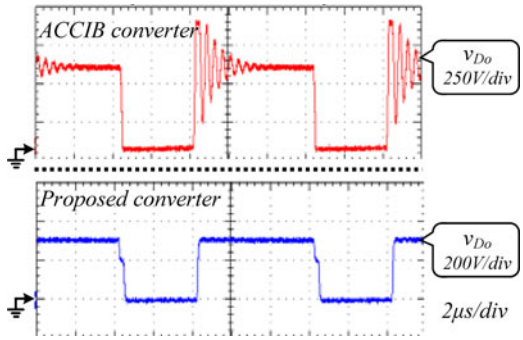

Fig. 17. Output diode voltage stress comparison between proposed converter and ACCIB converter.

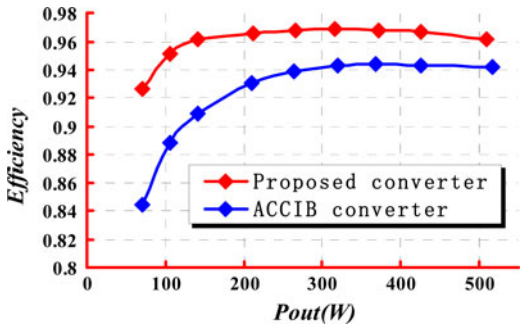

Fig. 18. Efficiency comparison between proposed converter and ACCIB converter.

turns OFF, the voltage of the main switch is clamped to that of the clamp capacitor. Thus, the turn-off voltage spikes of the main switch are suppressed greatly. The voltage stress of the main switch is about 150 V, which is far lower than the output voltage.

The gate-source voltage, drain-source voltage, and current waveforms of the main and clamp switches are shown in Figs. 14 and 15, respectively. ZVS turn-on conditions are realized for both the main and the clamp switches during the whole switching cycle, which reduces the switching losses greatly.

The voltage and current waveforms of the output diode and the regenerative diode are illustrated in Fig. 16. It is shown that the voltage stresses of these two diodes are equal to the output voltage.

The experimental results comparison of the output diode voltages between the proposed converter and ACCIB converter are shown in Fig. 17. The resonance between the leakage inductance and the stray capacitor of the output diode exists in the ACCIB converter, which increases the voltage stress of the output diode and causes additional losses on the diode. Although a RCD snubber is employed to solve the problem, the voltage stress of the output diode is still higher than 750 V. The voltage stress can be reduced by adjusting the parameter of the snubber, but the losses on the snubber are increased in that case. Fortunately, in the proposed converter, the voltage stress of the output diode is 380 V, and there are no voltage spikes on the diode. Low forward voltage drop diode can be used to improve the efficiency.

The measured efficiency comparison at different loads between the proposed converter and the ACCIB converter is shown in Fig. 18. The highest efficiency of the proposed converter is 96.9%, and the efficiency is higher than 96% over a wide load range. Compared with the ACCIB converter, there is about 2% efficiency improvement at full load and about 6% efficiency improvement at light load. The losses on the RCD snubber in the ACCIB converter are about 4.7 W, which is almost constant and not relative to the load condition. Therefore, it accounts for about 0.9% losses at full load and approximately 5% losses at light load. Though a lossless snubber can be applied to cancel the clamp losses, the complexity of the converter will increase, and this converter will have even more components than the proposed converter.

VI. Conclusion

A single-phase improved ACCIB converter with extended voltage doubler cell for high step-up applications has been presented in this paper to boost the relative low output voltage of the PV panel to supply the grid. By introducing the extended voltage doubler cell, which consists of a coupled inductor, a switched capacitor and a diode, the voltage stress of the switch is reduced greatly, and low voltage rated, low on-resistance, and high performance switch is adopted to reduce the conduction losses. Meanwhile, the active clamp circuit is applied to make all the switches work with ZVS-on condition and minimize the switching losses. Furthermore, the turn-off voltage spikes on the main switch are suppressed and the leakage inductance energy is recycled. The steady-state operational analysis and the main circuit performance are discussed to explore the advantages of the proposed converter. Finally, a 500 W prototype of the proposed converter has been built to verify the analysis and the experimental results have demonstrated that the proposed converter is an excellent power converter for high step-up applications without isolation requirement.

Appendix

By considering the leakage inductance of the coupled inductor, the voltage gain of the proposed converter is derived as follows.

The time intervals from t_1 to t_4 and from t_5 to t_8 are relatively short and cannot be considered in the voltage gain analysis. The ideal current waveform of the leakage inductance is taken as a straight line during each subinterval due to the relatively large resonant period. The simplified waveforms are shown in Fig. 19.

The whole switching period can be separated into two sections. During the section from t_1 to t_5, the main switch is in the OFF-state and the clamp switch is in the ON state. According to the current balance law, the average currents through the output diode and the regenerative diode are both equal to the load current. Therefore, the peak current of the output diode is given by

$$I_{Do\_\mathrm{peak}} = \frac{2 \cdot I_o}{1-D}. \tag{A1}$$

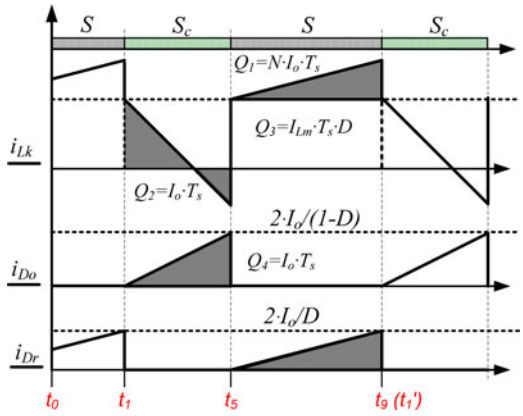

Fig. 19. Simplified waveforms.

And the voltage across the leakage inductance during this section can be derived

$$V_{Lk\_t15} = L_k \cdot \frac{N \cdot I_{Do\_\mathrm{peak}} \cdot f_s}{1-D} = \frac{2 \cdot N \cdot L_{Lk} \cdot I_o \cdot f_s}{(1-D)^2}. \tag{A2}$$

The output voltage is expressed by

$$V_{\mathrm{out}} = V_{Cc} + V_{Cm} + (V_{Cc} - V_{\mathrm{in}} - V_{Lk\_t15}) \cdot N. \tag{A3}$$

During the other section from t_5 to t_9, the main switch is in the ON state and the clamp switch is in the OFF state. The peak current of the regenerative diode and the voltage across the leakage inductance during this section are given by

$$I_{Dr\_\mathrm{peak}} = \frac{2 \cdot I_o}{D} \tag{A4}$$

$$V_{Lk\_t59} = L_k \cdot \frac{N \cdot I_{Dr\_\mathrm{peak}} \cdot f_s}{D} = \frac{2 \cdot N \cdot L_{Lk} \cdot I_o \cdot f_s}{D^2}. \tag{A5}$$

The voltage across the switched capacitor is expressed by

$$V_{Cm} = N \cdot (V_{\mathrm{in}} - V_{Lk\_59}). \tag{A6}$$

In addition, by applying the inductor volt-second balance principle, the voltage across the clamp capacitor can be obtained, which is given by

$$V_{Cc} = \frac{1}{1-D} \cdot V_{\mathrm{in}}. \tag{A7}$$

From (A2), (A3), and (A5)–(A7), the voltage gain expression can be calculated out as follows:

$$M = \frac{N+1}{1-D} \cdot \frac{1}{1 + 2 \cdot k_m \cdot N^2/D^2 + 2 \cdot k_m \cdot N^2/(1-D)^2} \tag{A8}$$

where $k_m = L_{Lk} \cdot f_s / R_o$.

References

[1] H. Patel and V. Agarwal, "MATLAB-based modeling to study the effects of partial shading on PV array characteristics," *IEEE Trans. Energy Convers.*, vol. 23, no. 1, pp. 302–310, Mar. 2008.

[2] E. Roman, R. Alonso, P. Ibanez, S. Elorduizapatarietxe, and D. Goitia, "Intelligent PV module for grid-connected PV systems," *IEEE Trans. Ind. Electron.*, vol. 53, no. 4, pp. 1066–1073, Jun. 2006.

[3] J. M. Kwon, B. H. Kwon, and K. H. Nam, "High-efficiency module-integrated photovoltaic power conditioning system," *IET Trans. Power Electron.*, vol. 2, no. 4, pp. 1755–4535, Jul. 2009.

[4] Q. Li and P. Wolfs, "A review of the single phase photovoltaic module integrated converter topologies with three different DC link configurations," *IEEE Trans. Power Electron.*, vol. 23, no. 3, pp. 1320–1333, May 2008.
[5] W. Li and X. He, "ZVT interleaved boost converters for high-efficiency, high step-up DC-DC conversion," *IET Trans. Power Electron.*, vol. 1, no. 2, pp. 284–290, Mar. 2007.
[6] R. J. Wai, C. Y. Lin, R. Y. Duan, and Y. R. Chang, "High-efficiency DC–DC converter with high voltage gain and reduced switch stress," *IEEE Trans. Ind. Electron.*, vol. 54, no. 1, pp. 354–364, Feb. 2007.
[7] R. W. Erickson and D. Maksimovic, *Fundamentals of Power Electronics*, 2nd ed. Norwell, MA: Kluwer, 2001.
[8] J. M. Kwon, E. H. Kim, B. H. Kwon, and K. H. Nam, "High-efficiency fuel cell power conditioning system with input current ripple reduction," *IEEE Trans. Ind. Appl.*, vol. 56, no. 3, pp. 826–834, Mar. 2009.
[9] H. Zhou, A. M. Khambadkone, and X. Kong, "Passivity-based control for an interleaved current-fed full-bridge converter with a wide operating range using the Brayton–Moser form," *IEEE Trans. Power Electron.*, vol. 24, no. 9, pp. 2047–2056, Sep. 2009.
[10] Q. Li and P. Wolfs, "A current fed two-inductor boost converter with an integrated magnetic structure and passive lossless snubbers for photovoltaic module integrated converter applications," *IEEE Trans. Power Electron.*, vol. 22, no. 1, pp. 309–321, Jan. 2007.
[11] J. M. Kwon and B. H. Kwon, "High step-up active-clamp converter with input-current doubler and output-voltage doubler for fuel cell power systems," *IEEE Trans. Power Electron.*, vol. 24, no. 1, pp. 108–115, Jan. 2009.
[12] C. Leu and M. Li, "A novel current-fed boost converter with ripple reduction for high-voltage conversion applications," *IEEE Trans. Ind. Electron.*, vol. 57, no. 6, pp. 2018–2023, Jun. 2010.
[13] V. Vaisanen, T. Riipinen, and P. Silventoinen, "Effects of switching asymmetry on an isolated full-bridge boost converter," *IEEE Trans. Power Electron.*, vol. 25, no. 8, pp. 2033–3044, Aug. 2010.
[14] O. Abutbul, A. Gherlitz, Y. Berkovich, and A. Ioinovici, "Step-up switching-mode converter with high voltage gain using a switched-capacitor circuit," *IEEE Trans. Circuits Syst. I*, vol. 50, no. 8, pp. 1098–1102, Aug. 2003.
[15] K. K. Law, K. W. E. Cheng, and Y. P. B. Yeung, "Design and analysis of switched-capacitor-based step-up resonant converters," *IEEE Trans. Circuits Syst. I*, vol. 52, no. 5, pp. 943–948, May 2005.
[16] M. Prudente, L. L. Pfitscher, G. Emmendoerfer, E. F. Romaneli, and R. Gules, "Voltage multiplier cells applied to non-isolated DC–DC converters," *IEEE Trans. Power Electron.*, vol. 23, no. 2, pp. 871–887, Mar. 2008.
[17] B. Axelrod, Y. Berkovich, and A. Ioinovici, "Switched-capacitor/switched-inductor structures for getting transformerless hybrid DC–DC PWM converters," *IEEE Trans. Circuits Syst. I*, vol. 55, no. 2, pp. 687–696, Mar. 2008.
[18] A. A. Fardoun and E. H. Ismail, "Ultra step-up DC–DC converter with reduced switch stress," *IEEE Trans. Ind. Appl.*, vol. 46, no. 5, pp. 2025–2034, Sep. 2009.
[19] L. Yang, T. Liang, and J. Chen, "Transformerless DC–DC converters with high step-up voltage gain," *IEEE Trans. Ind. Electron.*, vol. 56, no. 8, pp. 3144–3152, Aug. 2009.
[20] F. A. Himmelstoss and P. H. Wurm, "Low-loss converters with high step-up conversion ratio working at the border between continuous and discontinuous mode," in *Proc. IEEE Int. Conf. Electron., Circuits, Systems (ICECS) 2000*, pp. 734–737.
[21] Q. Zhao and F. C. Lee, "High-efficiency, high step-up DC-DC converters," *IEEE Trans. Power Electron.*, vol. 18, no. 1, pp. 65–73, Jan. 2003.
[22] K. C. Tseng and T. J. Liang, "Novel high-efficiency step-up converter," *IEE Proc. Electric Power Appl.*, vol. 151, no. 2, pp. 182–190, Mar. 2004.
[23] R. J. Wai and R. Y. Duan, "High-efficiency DC/DC converter with high voltage gain," *IEE Proc. Electric Power Appl.*, vol. 152, no. 4, pp. 793–802, Jul. 2005.
[24] R. J. Wai and R. Y. Duan, "High step-up converter with coupled-inductor," *IEEE Trans. Power Electron.*, vol. 20, no. 5, pp. 1025–1035, Sep. 2005.
[25] J. W. Baek, M. H. Ryoo, T. J. Kim, D. W. Yoo, and J. S. Kim, "High boost converter using voltage multiplier," in *Proc. IEEE 31st Ann. Conf. Ind. Electron Soc. (IECON)*, 2005, pp. 567–572.
[26] T. F. Wu, Y. S. Lai, J. C. Hung, and Y. M. Chen, "Boost converter with coupled inductors and buck–boost type of active clamp," *IEEE Trans. Ind. Electron.*, vol. 55, no. 1, pp. 154–162, Jan. 2008.

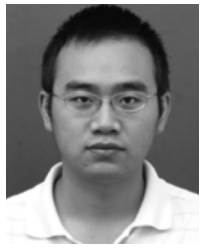

Yi Zhao (S'10) was born in Liaoning, China, in 1983. He received the B.Sc. degree from the College of Electrical and Electronic Engineering, Huazhong University of Science and Technology, Wuhan, China, in 2006. He is currently working toward the Ph.D. degree at the College of Electrical Engineering, Zhejiang University, Hangzhou, China.

His research interests include dc–dc converters and photovoltaic power system.

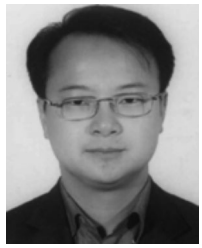

Wuhua Li (M'09) received the B.Sc. and Ph.D. degrees in applied power electronics and electrical engineering from Zhejiang University, Hangzhou, China, in 2002 and 2008, respectively.

From September 2004 to March 2005, he was an Intern, and from January 2007 to June 2008, a Research Assistant at the GE Global Research Center, Shanghai, China. From July 2008 to April 2010, he was a Postdoctoral Fellow at the College of Electrical Engineering, Zhejiang University. In May 2010, he became a faculty member at Zhejiang University as a Lecturer. In December 2010, he was promoted to Associate Professor. From July 2010 to September 2011, he was a Ryerson University Postdoctoral Fellow with the Department of Electrical and Computer Engineering, Ryerson University, Toronto, ON, Canada. He has published more than 70 technical papers and holds more than 20 issued/pending patents. His research interests include high-efficiency power converters and renewable energy power conversion system.

Xiangning He (M'95–SM'96–F'10) received the B.Sc. and M.Sc. degrees from the Nanjing University of Aeronautical and Astronautical, Nanjing, China, in 1982 and 1985, respectively, and the Ph.D. degree from Zhejiang University, Hangzhou, China, in 1989.

From 1985 to 1986, he was an Assistant Engineer at the 608 Institute of Aeronautical Industrial General Company, Zhuzhou, China. From 1989 to 1991, he was a Lecturer at Zhejiang University. In 1991, he obtained a Fellowship from the Royal Society of U.K., and conducted research in the Department of Computing and Electrical Engineering, Heriot-Watt University, Edinburgh, U.K., as a Postdoctoral Research Fellow for two years. In 1994, he joined Zhejiang University as an Associate Professor. Since 1996, he has been a Full Professor at the College of Electrical Engineering, Zhejiang University. He was the Director of the Power Electronics Research Institute and the Head of the Department of Applied Electronics, and he is currently the Vice Dean of the College of Electrical Engineering, Zhejiang University. He is the author or coauthor of more than 200 papers and one book *Theory and Applications of Multi-level Converters*, China Machine Press, 2006. He holds 12 patents. His research interests include power electronics and their industrial applications.

Dr. He received the 1989 Excellent Ph.D. Graduate Award, the 1995 Elite Prize Excellence Award, the 1996 Outstanding Young Staff Member Award, and the 2006 Excellent Staff Award from Zhejiang University for his teaching and research contributions. He received five Scientific and Technological Progress Awards from the Zhejiang Provincial Government and the State Educational Ministry of China in 1998, 2002, and 2009, respectively, and five Excellent Paper Awards. He is a Fellow of the Institution of Engineering and Technology (formerly IEE), U.K.